Front. Energy 2025, 19(6): 1037–1044
https://doi.org/10.1007/s11708-025-1001-9

RESEARCH ARTICLE

Molecular iron phthalocyanines anchoring onto ZIF-67-derived cobalt-carbon nanomaterials as bifunctional oxygen catalysts

Xiaoyu Lin[1], Deli Lin[1], Weiwu Zhang[1], Jie Liu[3], Yanqiong Shen (✉)[2], Jinjie Qian (✉)[3]

1 State Grid Wencheng Electric Power Supply Company, Wenzhou 325300, China
2 College of Chemistry and Chemical Engineering, Zhaotong University, Zhaotong 657000, China
3 College of Chemistry and Materials Engineering, Wenzhou University, Wenzhou 325035, China

Abstract Both oxygen reduction reaction (ORR) and oxygen evolution reaction (OER) are crucial for advancing the industrial application of fuel cells and metal-air batteries. This paper reports a bifunctional oxygen catalyst (CoNC@FePc) synthesized by anchoring FePc molecules onto cobalt nanoparticles embedded within a Co-ZIF-derived nitrogen-doped carbon matrix (CoNC). By leveraging the significant electron transfer between Co nanoparticles and FePc molecules, the synthesized catalyst demonstrated outstanding performance for both ORR and OER, further validated by density functional theory (DFT) calculations. The catalyst achieved a half-wave potential of 0.87 V for ORR and a low overpotential of 314 mV at 10 mA/cm^2 for OER, surpassing the performance of commercial Pt/C and RuO_2, respectively. Additionally, the rechargeable zinc-air batteries incorporating CoNC@FePc exhibited a remarkable peak power density of 150.2 mW/cm^2 and maintained outstanding cyclic stability for over 100 h. This study offers a straightforward approach to improving the bifunctional oxygen electrocatalytic performance of metal phthalocyanine-based catalysts.

Keywords metal-organic framework, Fe phthalocyanine, Co nanoparticle, carbon material, oxygen catalyst

1 Introduction

As global energy demands continue to rise, coupled with growing concerns over the depletion of fossil fuel reserves, the development of cost-effective, sustainable, and environmentally friendly energy technologies has become a critical area of focus. Rechargeable zinc-air batteries (RZABs) have emerged as a promising solution owing to their exceptional properties, including high energy density, the widespread availability of zinc, and environmental compatibility. These characteristics position RZABs as a viable candidate for addressing the dual challenges of energy scarcity and environmental pollution, thus offering a renewable, efficient, and eco-friendly alternative for future energy storage systems [1–4]. Additionally, compared to fuel cells, RZABs offer improved safety, exceptional flexibility for wearable devices, and the ability to be recharged, making them an ideal energy source for portable electronic devices [5,6]. However, the sluggish reaction kinetics and inferior structural durability of the oxygen reduction reaction (ORR) and oxygen evolution reaction (OER) remain significant challenges for the large-scale utilization of RZABs [7–9]. To enhance the practical viability of ZABs, the rational design and development of high-performance catalysts that facilitate rapid electron and mass transfer, reduce reaction energy barriers, and improve energy efficiency is essential. Currently, the most advanced ORR and OER electrocatalysts are primarily composed of noble metals, such as Pt/C and RuO_2, and their varied derivatives [10]. Nonetheless, their inherent limitations, such as poor stability and high costs, substantially hinder their practical applications in the energy sector [11,12]. Thus, the development of inexpensive, efficient, and durable catalysts is crucial for the widespread commercialization of RZABs.

Received Dec. 15, 2024; accepted Mar. 3, 2025; online Mar. 30, 2025
Correspondences: Yanqiong Shen, shenyq@ztu.edu.cn;
Jinjie Qian, jinjieqian@wzu.edu.cn

Multifunctional metal-nitrogen-carbon single-atom catalysts (M-N-C SACs) have emerged as highly promising candidates for both ORR and OER, owing to their outstanding atomic utilization, excellent catalytic selectivity, tunable electronic structures, and high electrical conductivity [13–17]. In this regard, metal phthalocyanines (MPcs), representative macrocyclic M-N-C-based molecules, have gained recognition as effective molecular catalysts for ORR due to their straightforward synthesis and remarkable catalytic performance [18–21]. However, these molecular catalysts require highly specific carbon substrates, such as single-/multi-walled carbon nanotubes, 2D graphene, and porous carbons, to achieve satisfactory electrocatalytic performance [22,23]. It is important to note that most carbon-based heterogeneous catalysts exhibit limited stability during charging–discharging cycles and under high-voltage conditions in practical applications. The corrosion of carbon nanomaterials plays a key role in activity degradation and reduced lifespan during electrocatalytic oxidation, resulting in the aggregation, dissolution, and detachment of the embedded metal active centers [24]. Therefore, the design and preparation of suitable carbon substrates to anchor FePc molecules for achieving efficient and stable bifunctional ORR and OER performance remains a significant challenge.

Recently, metal-organic frameworks (MOFs) have attracted significant attention in electrocatalysis due to their adaptable and customizable nanostructures, exceptionally high surface area, and abundant porosity [25–27]. Among various MOFs, zeolitic imidazolate frameworks (ZIFs) are particularly notable as a subclass of crystalline inorganic-organic hybrids with high nitrogen content. Through a straightforward pyrolysis process, ZIFs can be easily converted into hierarchically porous carbon nanomaterials with uniformly doped metal-nitrogen sites [28,29]. Additionally, Co-based ZIFs are particularly effective in deriving active species (such as Co nanoparticles (NPs) [30], Co_3O_4 [31], CoP [32], CoS_x [33]) for OER. Inspired by these advantages, a bifunctional CoNC@FePc was successfully synthesized using a straightforward pyrolysis method, based on the Co-ZIF precursor. In this process, FePc molecules were loaded onto Co NPs within an N-doped carbon substrate via a convenient solution-based approach (Fig. 1). Thanks to the strong molecular interaction between FePc molecules and Co species, the resulting catalyst exhibited superior bifunctional oxygen catalytic performance, achieving a positive half-wave potential of 0.87 V for ORR and a minimal overpotential for OER. Moreover, the assembled ZAB using CoNC@FePc as the air cathode exhibited an impressive open-circuit potential of 1.53 V and a peak power density of 150.2 mW/cm^2. It also demonstrated excellent electrochemical and structural stability, maintaining consistent performance over a charge–discharge cycling of approximately 100 h.

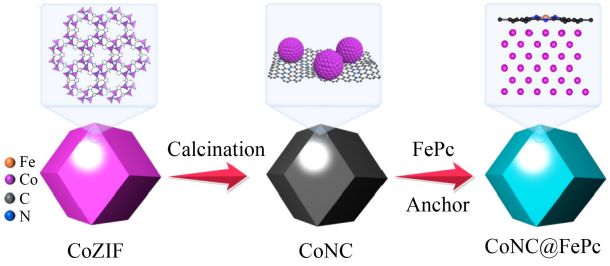

Fig. 1 Schematic preparation of bifunctional CoNC@FePc for ORR/OER.

2 Results and discussion

To investigate the morphology of CoNC@FePc, scanning electron microscopy (SEM) and transmission electron microscopy (TEM) were employed. The SEM images provided detailed insights into the structural features of CoNC@FePc, revealing that its morphology largely retained the features of the Co-ZIF precursor (Figs. S1–S3). Figures 2(a) and 2(b) present the TEM and high-resolution TEM (HRTEM) images, clearly revealing the hexagonal morphology of CoNC. The HRTEM image displayed two distinct fringe lattices of 0.336 and 0.205 nm, attributed to the graphitic C (002) and metallic Co (111) planes, respectively [34]. Additionally, the aberration-corrected annular dark-field scanning transmission electron microscopy (AC-HAADF-STEM) image (Fig. 2(c)) revealed a pronounced concentration of bright spots within the material. These spots were indicative of atomically dispersive FePc molecules and the *in-situ* formation of Co species. Larger bright spots corresponded to Co NPs, while the smaller isolated bright spots were consistent with individual FePc molecules. This distinctive imaging pattern confirmed the presence of Co NPs and FePc molecules, both embedded on the porous graphitic N-doped carbon substrate.

In Fig. 2(d), the powder X-ray diffraction (PXRD) analysis of CoNC@FePc revealed diffraction patterns similar to those of CoNC. Specifically, two prominent peaks were observed at 44.09° and 51.37°, corresponding to the (111) and (200) crystallographic planes of metallic cobalt (PDF #97-005-3805). Remarkably, no distinct diffraction peaks associated with FePc were detected after it was dispersed and anchored onto the porous CoNC, indicating that FePc species remained well-dispersed without noticeable aggregation. This suggests that the interaction between FePc molecules and the CoNC matrix effectively prevented the formation of larger aggregates. Furthermore, energy-dispersive X-ray spectroscopy (EDS) and corresponding elemental mapping confirmed the uniform distribution of C, N, O, Co, and Fe across the ZIF-derived carbon substrate (Fig. 2(e), Fig. S4).

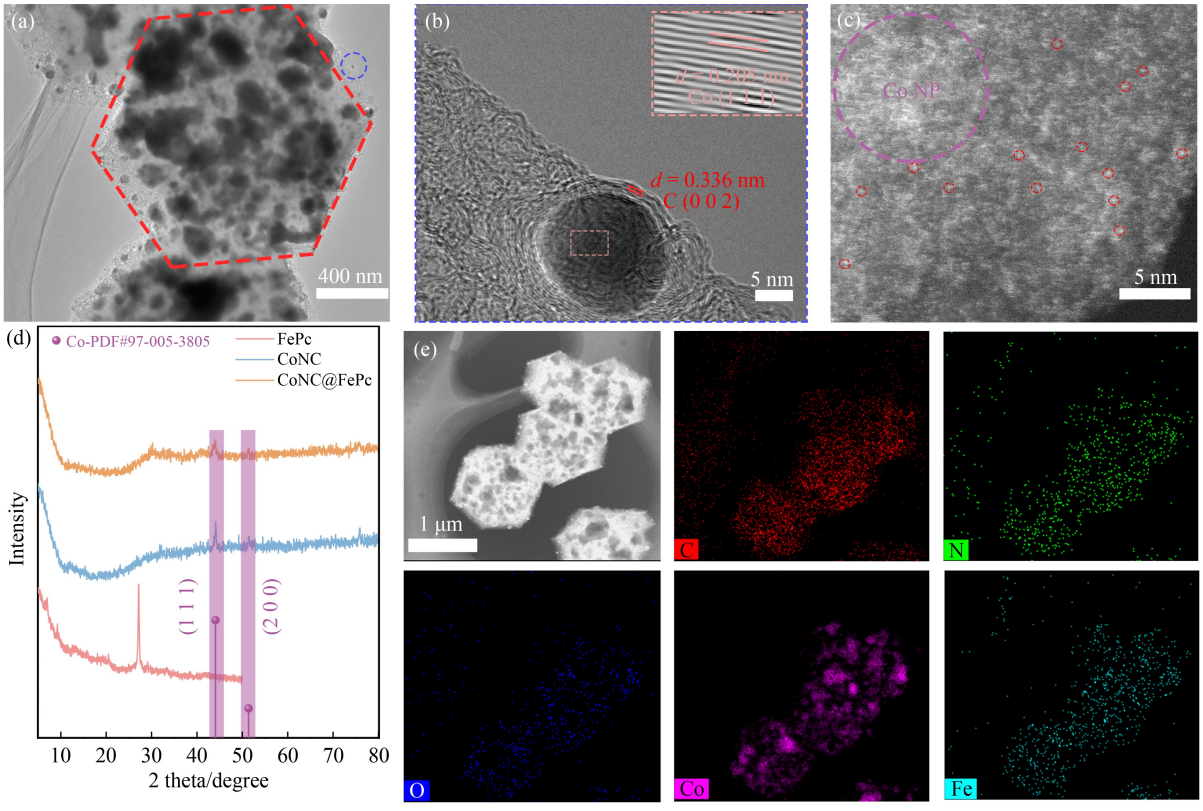

Fig. 2 Morphology and phase characterization.
(a) TEM image; (b) HRTEM image; (c) HAADF-STEM image of CoNC@FePc; (d) PXRD patterns; (e) EDS mapping images.

The nitrogen adsorption–desorption isotherms of MOF-derived CoNC exhibited typical type-IV behavior, indicative of the presence of abundant mesoporosity and a substantial surface area of 106.2 m^2/g (Fig. 3(a)). However, upon incorporation of molecular catalysts of FePc into the porous CoNC framework, the surface area of the resulting CoNC@FePc composite significantly decreased to 34.2 m^2/g. This reduction suggests that the FePc molecules have effectively infiltrated and occupied the mesopores of the CoNC, as summarized in Table S1. Raman spectra (Fig. 3(b)) clearly confirmed the presence of FePc, with two distinct peaks at 1390.83 and 1506.62 cm^{-1}, characteristic of FePc's molecular vibrations [35]. In addition, two more significant peaks at 1331 and 1577 cm^{-1} were observed, corresponding to the D band and G band of the carbon material, respectively. The relative intensity ratio (I_D/I_G) of the D to G bands was calculated to be 1.09 for CoNC@FePc and 0.98 for CoNC, suggesting a higher level of disorder and an increased concentration of defects in the CoNC@FePc composite. This enhanced structural disorder in CoNC@FePc, compared to CoNC, reflects the incorporation of FePc and its impact on the carbon matrix [36].

The high-resolution C 1s XPS spectra (Fig. 3(c)) were carefully deconvoluted into four subpeaks, corresponding to different carbon species: O–C = O at 292.3 eV, C–O at 289.6 eV, C–N at 287.1 eV, and C–C at 284.8 eV. Similarly, the deconvoluted N 1s spectra (Fig. 3(d)) revealed four nitrogen species within the CoNC@FePc structure: oxidized nitrogen at 404.1 eV, graphitic nitrogen at 402.1 eV, pyrrolic nitrogen at 400.4 eV, and pyridinic nitrogen at 398.9 eV (Table S2). The high-resolution spectra of Co $2p_{3/2}$ and Co $2p_{1/2}$ peaks, shown in Fig. 3(e), appeared at binding energies of 777.6/792.3, 781.0/796.5, 784.8/800.5, and 788.0/804.0 eV, corresponding to Co(0), Co(III), Co(II), and satellite peaks, respectively. Importantly, the Co $2p_{3/2}$ peak shifted significantly by 0.9 eV to higher binding energies, suggesting effective charge redistribution between the Co species and the molecular FePc catalysts. This shift likely reflected the establishment of strong electronic interactions, enhancing charge transfer and potentially influencing the electronic structure and catalytic performance of the CoNC@FePc composite.

The electrochemical performance of CoNC@FePc was systematically evaluated using a rotating ring-disk electrode (RRDE). As illustrated in Figs. 4(a) and S7, the linear sweep voltammetry (LSV) curves showed that the optimal CoNC@FePc exhibited a superior half-wave potential ($E_{1/2}$) of 0.87 V, alongside a high diffusion-limiting current (J_L) of 5.42 mA/cm^2. These values notably outperform those of Pt/C ($E_{1/2}$= 0.85 V, J_L = 5.24 mA/cm^2) and CoNC ($E_{1/2}$ = 0.79 V, J_L =

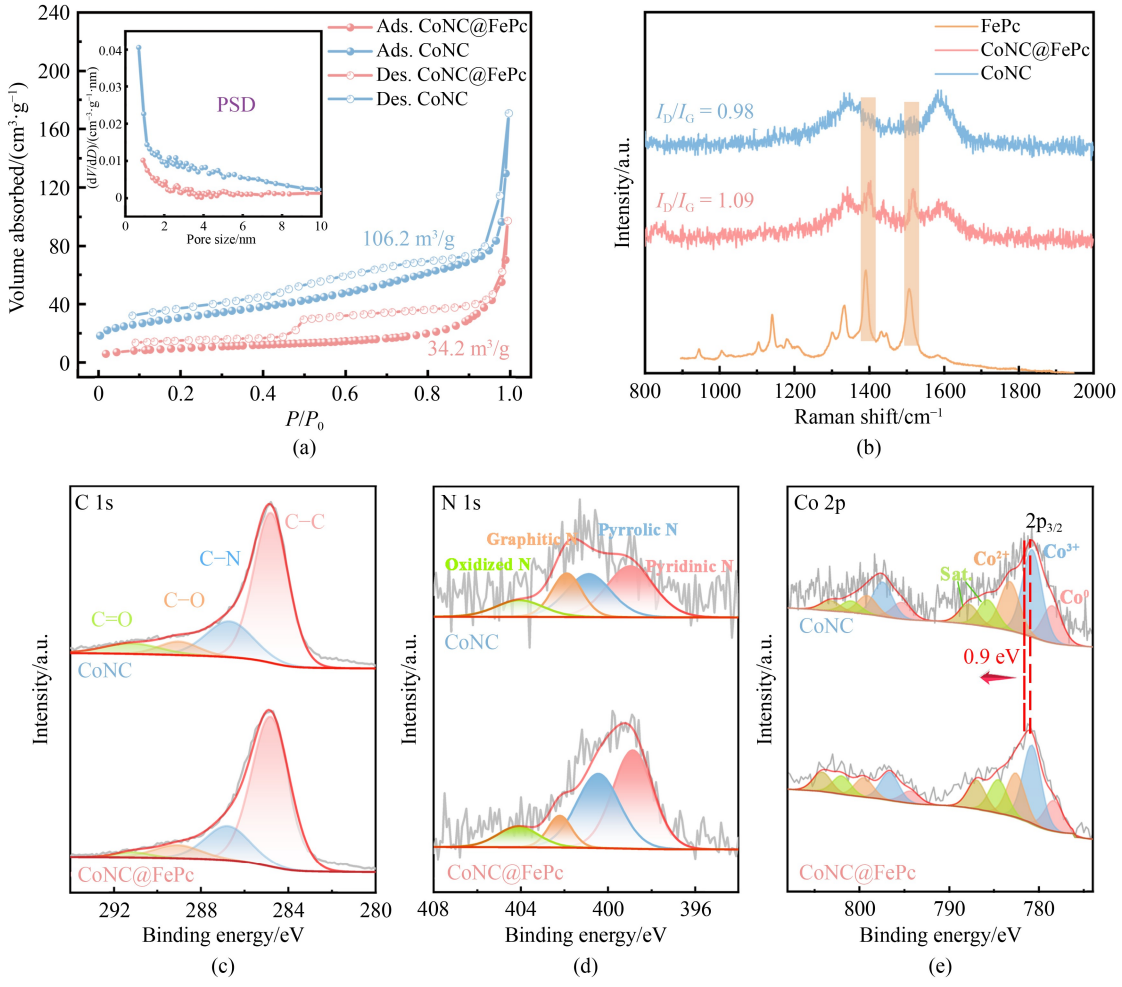

Fig. 3 BET/Raman/XPS data.

(a) N_2 isotherms; (b) Raman spectra; (c) the deconvoluted XPS spectra of C 1s; (d) deconvoluted XPS spectra of N 1s; (e) deconvoluted XPS spectra of Co 2p.

4.11 mA/cm^2), highlighting the enhanced catalytic performance and electrochemical activity of CoNC@FePc. The Tafel slope for CoNC@FePc was calculated to be 38.8 mV/dec, significantly lower than those for CoNC (53.3 mV/dec) and Pt/C (91.1 mV/dec), indicating much faster kinetic efficiency for ORR (Fig. 4(b)).

The ORR pathway selectivity, depicted in Fig. 4(c), revealed that CoNC@FePc effectively facilitated the preferred 4-electron transfer pathway, minimizing the formation of hydrogen peroxide (H_2O_2). To assess the electrochemical active surface area (ECSA), the electrochemical double-layer capacitance (C_{dl}) was measured. CoNC@FePc demonstrated the largest Cdl value of 23.1 cm^{-2}, surpassing both CoNC (20.2 mF/cm^2) and Pt/C (14.8 mF/cm^2), as shown in Fig. 4(d). This indicates that CoNC@FePc possesses a significantly larger electrochemically accessible surface area, contributing to its enhanced catalytic activity.

Furthermore, upon the introduction of a methanol (MeOH) solution, CoNC@FePc exhibited only a minor change in current density (8.7%), in sharp contrast to the more substantial decrease observed for Pt/C (18.1%) (Fig. 4(e)). After a 16-h electrochemical evaluation, CoNC@FePc retained 95.4% of its initial current density, a performance significantly superior to Pt/C, which maintained only 88.3% (Fig. 4(f)). This substantial retention of current density underscores the exceptional long-term stability of CoNC@FePc.

Regarding the OER performance, CoNC@FePc demonstrated a low overpotential (η_{10}) of 314 mV at a current density of 10 mA/cm^2, outperforming both RuO_2 (331 mV) and CoNC (377 mV) (Fig. 4(g)). The calculated Tafel slope for CoNC@FePc was 73.4 mV/dec, significantly lower than the values for RuO_2 (143.8 mV/dec) and CoNC (91.2 mV/dec), suggesting faster reaction kinetics and superior catalytic efficiency for OER (Fig. 4(h)). Additionally, the excellent bifunctional catalytic activity of CoNC@FePc was confirmed by its narrow voltage gap (ΔE) of 0.679 V,

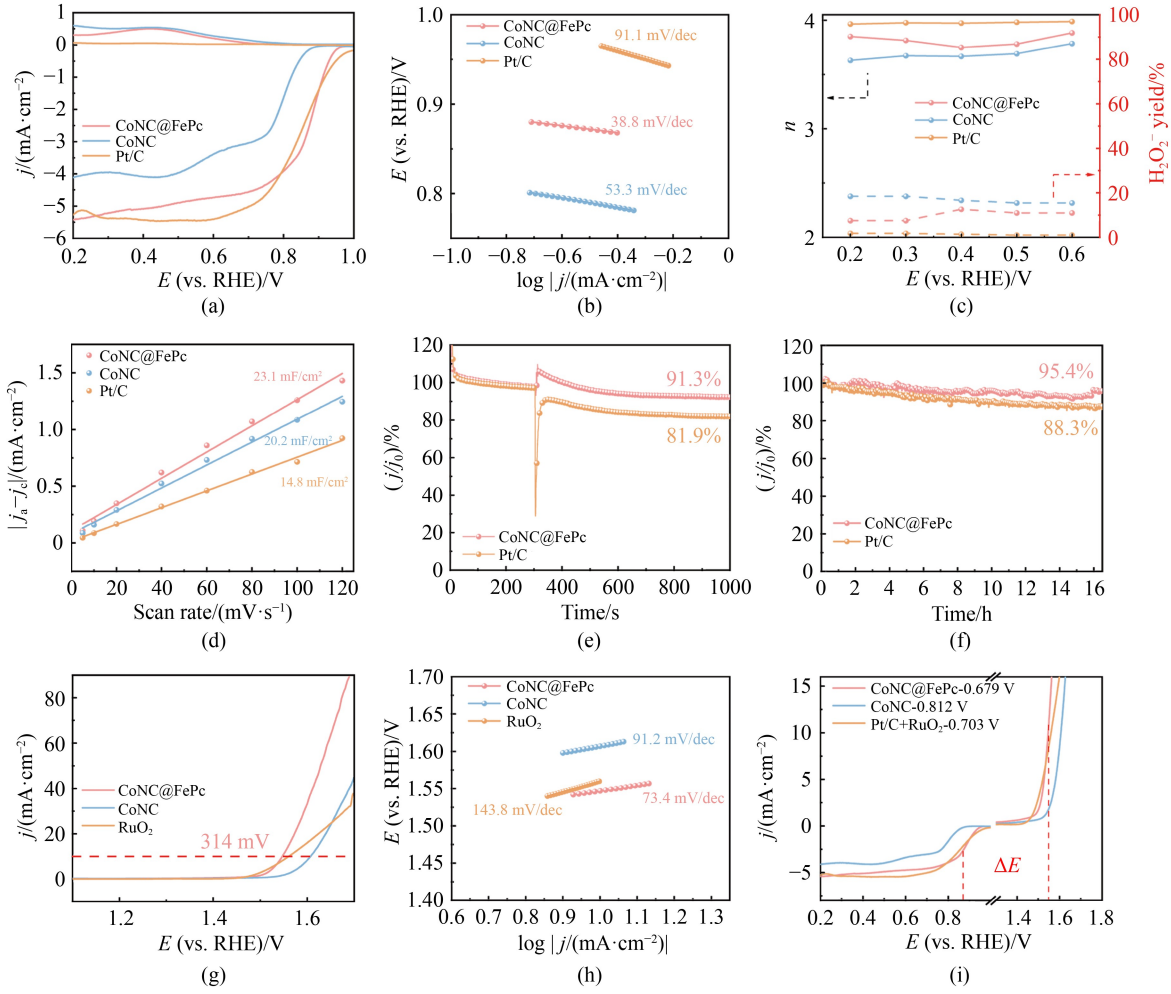

Fig. 4 ORR/OER data.

(a) LSV curves at 1600 r/min; (b) Tafel slopes; (c) *n* and H_2O_2 yields; (d) C_{dl} profiles; (e) MeOH tolerance test; (f) long-term durability test; OER test in 1 mol/L KOH; (g) LSV curves 1600 r/min, (h) Tafel slopes, (i) bifunctional electrocatalytic activities toward ORR and OER.

outperforming the Pt/C+RuO_2 pair (0.703 V), CoNC (0.812 V), and other benchmark electrocatalysts (Fig. 4(i), Table S3). These results collectively highlight CoNC@FePc as a highly efficient and durable electrocatalyst for both oxygen reduction and OERs.

To evaluate the practical viability of the as-synthesized catalysts, a series of zinc-air batteries (ZABs) were assembled. As shown in Fig. 5(a), the open circuit voltage (OCV) of CoNC@FePc-based ZABs was 1.53 V, outperforming the Pt/C-based ZABs (1.47 V). Moreover, the specific discharge capacity and energy density of CoNC@FePc-based ZABs were substantially higher, reaching 846.5 mAh/g Zn, compared to Pt/C, which exhibited 691.2 mAh/g Zn (Fig. 5(b)). In Fig. 5(c), the assembled CoNC@FePc-based ZABs demonstrated an impressive peak power density of 150.2 mW/cm^2, substantially exceeding that of the commercial Pt/C-based ZABs (139.7 mW/cm^2). Under identical operational conditions, the optimized CoNC@FePc-based batteries consistently delivered higher output voltages across a broad range of discharge current densities, highlighting their outstanding rate capability and stability at varying loads (Fig. 5(d)).

Figure 5(e) illustrated the discharge–charge cycling profiles of both ZAB types at a constant current density of 10 mA/cm^2. Notably, the CoNC@FePc-based ZAB exhibited a remarkably narrow voltage gap of 0.747 V, with charging and discharging voltages of 1.968 and 1.221 V, respectively, over an extended period of 100 h. In contrast, the commercial Pt/C+RuO_2-based ZAB demonstrated significantly lower cycling stability, with a limited operational lifespan of only 35 h. This substantial difference highlights the exceptional cycling stability and energy efficiency of CoNC@FePc-based ZABs, emphasizing their potential for high-performance, long-duration energy storage applications.

To gain a deeper insight into the intrinsic catalytic behaviors of FePc molecules on Co nanoparticle

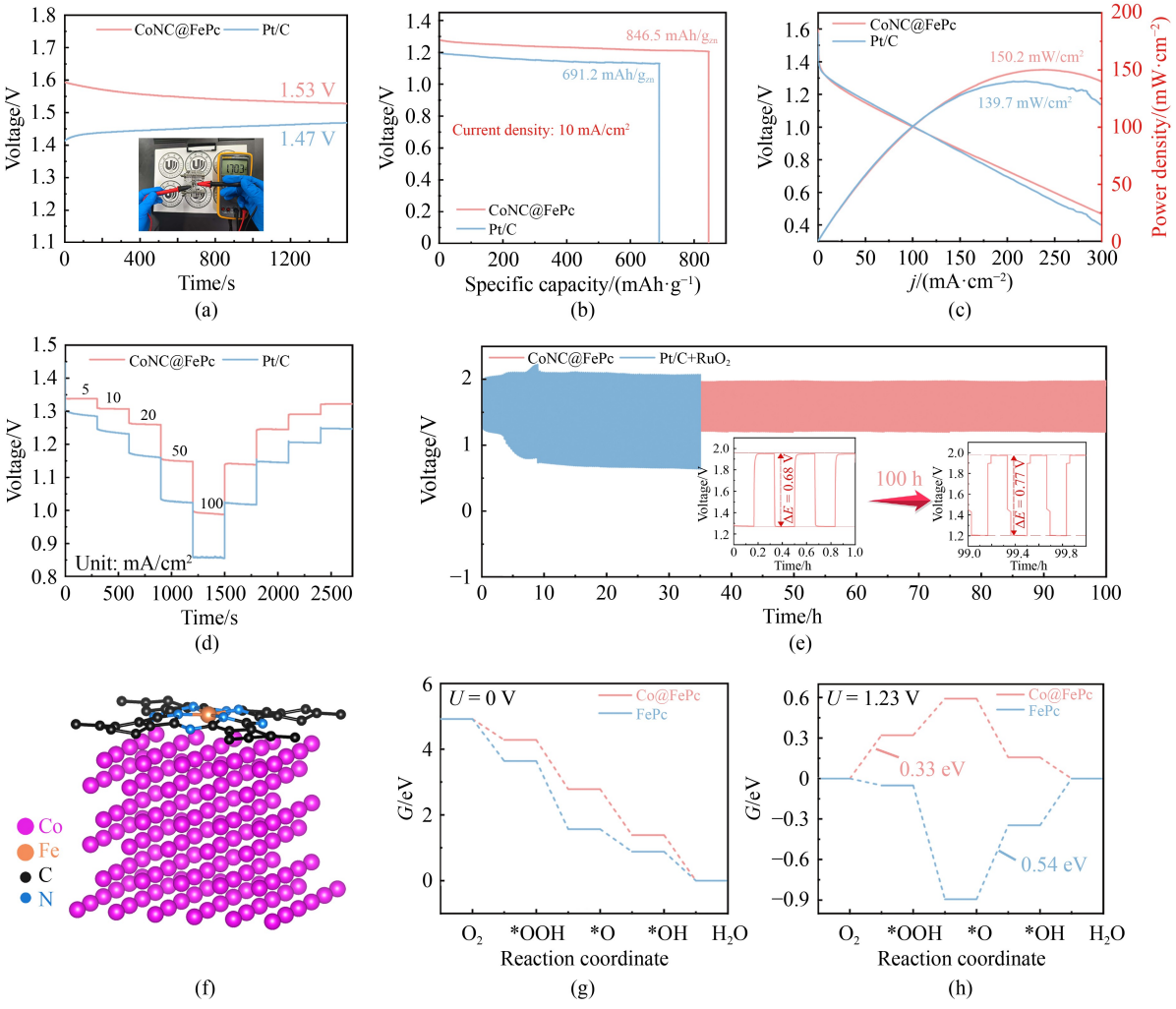

Fig. 5 ZAB test and DFT data.

(a) OCV plots of home-made ZAB; (b) galvanostatic discharge curves; (c) discharge polarization curves and corresponding power output density graphs; (d) discharge voltages at various current densities; (e) galvanostatic cycling profiles for CoNC@FePc and Pt/C + RuO_2; (f) model of Co@FePc; (g) ORR free energy diagrams at 0.00 V; (h) ORR free energy diagrams at 1.23 V.

substrates for ORR, density functional theory (DFT) calculations were performed. In the computational model depicted in Figs. 5(f) and S11, an FePc molecule was directly anchored to the Co (001) lattice plane, constructing the Co@FePc model. The ORR and OER pathways were modeled to involve four consecutive proton-coupled electron transfer steps, each step associated with the formation of reaction intermediates (Fig. S12) [37]. At an applied potential of 0.00 V, all the reaction steps displayed a favorable downhill free energy profile, indicating that both catalysts exhibit promising catalytic activity (Fig. 5(g)).

As shown in Fig. 5(h), the rate-determining step (RDS) for Co@FePc was identified as the reduction of $*O_2$ to *OOH, with a theoretical overpotential of 0.33 eV. This value is significantly lower than the RDS for FePc, which is the reduction of *O to *OH, with an overpotential of 0.54 eV. In the context of OER (Fig. S13), the RDS for Co@FePc was the conversion of *OH to *O, exhibiting a markedly lower energy barrier of 0.44 eV compared to FePc, which has an energy barrier of 0.84 eV. These results not only reinforce the superior ORR/OER performance of Co@FePc, but also provide critical insights into its enhanced catalytic efficiency.

3 Conclusions

In conclusion, FePc molecules were successfully anchored onto Co NPs within an N-doped carbon substrate through direct pyrolysis of Co-ZIF precursors. Owing to the electron interactions between Fe sites in FePc and Co NPs, the as-synthesized CoNC@FePc exhibited excellent bifunctional properties for both ORR and OER, achieving an $E_{1/2}$ potential of 0.87 V in a 0.1 mol/L KOH electrolyte and a low OER overpotential of 314 mV at a

current density of 10 mA/cm^2. The optimized CoNC@FePc catalyst was further employed in home-made ZABs, demonstrating a peak power density of 150.2 mW/cm^2 and exceptional charge and discharge cycling stability for over 100 h, outperforming the Pt/C + RuO_2 air cathode. The high activity of CoNC@FePc for bifunctional oxygen reactions was further confirmed by relevant theoretical calculations, where the RDS was identified as the conversion of *OH to *O for Co@FePc. This paper proposes a novel synthetic strategy for developing superior bifunctional oxygen electrocatalysts and offers significant potential for advancements in clean energy storage and conversion technologies.

Acknowledgements This work was financially supported by the Basic Science and Technology Research Project of Wenzhou, Zhejiang Province, China (No. G20240038), and the Special Basic Cooperative Research Programs of Yunnan Provincial Undergraduate Universities Association, China (Nos. 202301BA070001-093 and 202401BA070001-002).

Competing Interests The authors declare that they have no competing interests.

Electronic Supplementary Material Supplementary material is available in the online version of this article at https://doi.org/10.1007/s11708-025-1001-9 and is accessible for authorized users.

References

1. Shu X, Chen Q, Yang M, et al. Tuning Co-catalytic sites in hierarchical porous N-doped carbon for high-performance rechargeable and flexible Zn-air battery. Advanced Energy Materials, 2023, 13(1): 2202871
2. Liu J, Sun Q, Ye Q, et al. MOF-derived cobalt nanoparticles with dispersed iron phthalocyanines as bifunctional oxygen electrocatalysts. ACS Sustainable Chemistry & Engineering, 2024, 12(11): 4779–4788
3. Qiu Z, Guo X, Cao S, et al. High-entropy Ag−Ru-based electrocatalysts with dual-active-center for highly stable ultra-low-temperature zinc-air batteries. Angewandte Chemie International Edition, 2024, 64(3): e202415216
4. Mu C, Mao J, Guo J, et al. Rational design of spinel cobalt vanadate oxide Co_2VO_4 for superior electrocatalysis. Advanced Materials, 2020, 32(10): 1907168
5. Liu J N, Zhao C X, Wang J, et al. A data-driven bifunctional oxygen electrocatalyst with a record-breaking ΔE = 0.57 V for ampere-hour-scale zinc-air batteries. Joule, 2024, 8(6): 1804–1819
6. Zhang T, Bian J, Zhu Y, et al. FeCo nanoparticles encapsulated in N-doped carbon nanotubes coupled with layered double (Co, Fe) hydroxide as an efficient bifunctional catalyst for rechargeable zinc-air batteries. Small, 2021, 17(44): 2103737
7. Yang X, Su F, Hou M, et al. Plasma tailored reactive nitrogen species in MOF derived carbon materials for hybrid sodium–air batteries. Dalton Transactions, 2021, 50(20): 7041–7047
8. Yang X, Peng C, Hou M, et al. Rational design of electrolyte solvation structures for modulating $2e^-/4e^-$ transfer in sodium-air batteries. Advanced Functional Materials, 2022, 32(23): 2201258
9. Wang X T, Ouyang T, Wang L, et al. Redox-inert Fe^{3+} ions in octahedral sites of Co–Fe spinel oxides with enhanced oxygen catalytic activity for rechargeable zinc-air batteries. Angewandte Chemie International Edition, 2019, 58(38): 13291–13296
10. Ma Z, Cano Z P, Yu A, et al. Enhancing oxygen reduction activity of Pt-based electrocatalysts: From theoretical mechanisms to practical methods. Angewandte Chemie International Edition, 2020, 59(42): 18334–18348
11. Yuan C, Zhang S, Zhang J. Oxygen reduction electrocatalysis: From conventional to single-atomic platinum-based catalysts for proton exchange membrane fuel cells. Frontiers in Energy, 2024, 18(2): 206–222
12. Wang Z, Liu Y, Chen S, et al. Strain engineering of Pt-based electrocatalysts for oxygen reaction reduction. Frontiers in Energy, 2024, 18(2): 241–262
13. Wan X, Liu X, Li Y, et al. Fe-N-C electrocatalyst with dense active sites and efficient mass transport for high-performance proton exchange membrane fuel cells. Nature Catalysis, 2019, 2(3): 259–268
14. Liu K, Fu J, Lin Y, et al. Insights into the activity of single-atom Fe-N-C catalysts for oxygen reduction reaction. Nature Communications, 2022, 13(1): 2075
15. Han J, Bao H, Wang J Q, et al. 3D N-doped ordered mesoporous carbon supported single-atom Fe-N-C catalysts with superior performance for oxygen reduction reaction and zinc-air battery. Applied Catalysis B: Environmental, 2021, 280: 119411
16. Gong L, Jiang Z, Xiong Y, et al. Regulation the surface chemistry and electronic structure of Fe/Co/N co-doped hollow graphene spheres by different atmosphere plasma to enhance oxygen reduction/hydrogen evolution performance of loaded PtNi alloy nanoparticles. International Journal of Hydrogen Energy, 2023, 48(84): 32860–32874
17. Liu Y, Jiang Z, Jiang Z J. Plasma-assisted formation of oxygen defective NiCoO/NiCoN heterostructure with improved ORR/OER activities for highly durable all-solid-state zinc-air batteries. Advanced Functional Materials, 2023, 33(35): 2302883
18. Zhu S, Ding L, Zhang X, et al. Biaxially-strained phthalocyanine at polyoxometalate@carbon nanotube heterostructure boosts oxygen reduction catalysis. Angewandte Chemie International Edition, 2023, 62(42): e202309545
19. Yang Y, Sun Q, Xue J, et al. MOF-derived N-doped carbon nanosticks coupled with Fe phthalocyanines for efficient oxygen reduction. Chemical Engineering Journal, 2023, 464: 142668
20. Baker R, Wilkinson D P, Zhang J. Electrocatalytic activity and stability of substituted iron phthalocyanines towards oxygen reduction evaluated at different temperatures. Electrochimica Acta, 2008, 53(23): 6906–6919
21. He S, Wang J, Sun C. Boosted electrocatalytic activity and durability of CuFe/NC by modulating the interfacial composition and electronic structure for efficient oxygen reduction reaction. Journal of Colloid and Interface Science, 2025, 677: 771–780
22. Wang X, Wang B, Zhong J, et al. Iron polyphthalocyanine sheathed multiwalled carbon nanotubes: A high-performance electrocatalyst for oxygen reduction reaction. Nano Research, 2016, 9(5): 1497–1506

23. Cao R, Thapa R, Kim H, et al. Promotion of oxygen reduction by a bio-inspired tethered iron phthalocyanine carbon nanotube-based catalyst. Nature Communications, 2013, 4(1): 2076
24. Zhang S, Chen M, Zhao X, et al. Advanced noncarbon materials as catalyst supports and non-noble electrocatalysts for fuel cells and metal-air batteries. Electrochemical Energy Review, 2021, 4(2): 336–381
25. Li H, Eddaoudi M, O'Keeffe M, et al. Design and synthesis of an exceptionally stable and highly porous metal-organic framework. Nature, 1999, 402(6759): 276–279
26. Wang Y, Wu J, Tang S, et al. Synergistic Fe−Se atom pairs as bifunctional oxygen electrocatalysts boost low-temperature rechargeable Zn-air battery. Angewandte Chemie International Edition, 2023, 62(15): e202219191
27. Zhao L, Zhang J, Jin G, et al. Metal-organic framework-derived trimetallic particles encapsulated by ultrathin nitrogen-doped carbon nanosheets on a network of nitrogen-doped carbon nanotubes as bifunctional catalysts for rechargeable zinc-air batteries. Journal of Colloid and Interface Science, 2024, 668: 525–539
28. Zhu Y, Yue K, Xia C, et al. Recent advances on MOF derivatives for non-noble metal oxygen electrocatalysts in zinc-air batteries. Nano-Micro Letters, 2021, 13(1): 137
29. Shang N, Wang K, Wei M, et al. Challenges for large scale applications of rechargeable Zn-air batteries. Journal of Materials Chemistry. A, Materials for Energy and Sustainability, 2022, 10(31): 16369–16389
30. Lin M, Jiang D, Yan Y, et al. Temperature-controlled hydrothermal hydrogenation of palmitic acid to alkanol or alkanes over Co@CN–x catalysts derived from ZIF-67. Chemical Engineering Journal, 2024, 481: 148565
31. Wu J, Zheng Z, Chi H, et al. Ultrasensitive and exclusive chemiresistors with a ZIF-67-derived oxide cage/nanofiber Co_3O_4/In_2O_3 heterostructure for acetone detection. ACS Applied Materials & Interfaces, 2024, 16(7): 9126–9136
32. Sun Q, Liu J, Ji X, et al. Metal-organic framework derived hollow nitrogen-doped carbon sphere with cobalt phosphide in carbon nanotube for efficient oxygen evolution. Journal of Colloid and Interface Science, 2023, 652: 1338–1346
33. Chen Y, Rong J, Wu J, et al. MOF-derived S, N co-doped porous carbon matrix with single Fe atoms and CoS_x nanoparticles dual-sites for enhanced oxygen reduction. Chemical Engineering Journal, 2024, 502: 158080
34. Wang X, Dong A, Hu Y, et al. A review of recent work on using metal–organic frameworks to grow carbon nanotubes. Chemical Communications, 2020, 56(74): 10809–10823
35. Huang Z, Li M, Yang X, et al. Diatomic iron with a pseudo-phthalocyanine coordination environment for highly efficient oxygen reduction over 150000 cycles. Journal of the American Chemical Society, 2024, 146(36): 24842–24854
36. Ji X, Liu B, Ren X, et al. P-doped Ag nanoparticles embedded in N-doped carbon nanoflake: An efficient electrocatalyst for the hydrogen evolution reaction. ACS Sustainable Chemistry & Engineering, 2018, 6(4): 4499–4503
37. Nørskov J K, Rossmeisl J, Logadottir A, et al. Origin of the overpotential for oxygen reduction at a fuel-cell cathode. Journal of Physical Chemistry B, 2004, 108(46): 17886–17892